Study of the reactions occurring in the fusion of ^{12}C and ^{16}O with heavy nuclei at incident energies below 10 MeV/nucleon

M. Cavinato, E. Fabrici, E. Gadioli, E. Gadioli Erba, P. Vergani, M. Crippa, G. Colombo, I. Redaelli, and M. Ripamonti
Dipartimento di Fisica, Università di Milano, Istituto Nazionale di Fisica Nucleare, Sezione di Milano, I-20133 Milano, Italy
(Received 27 February 1995)

The excitation functions for production of many residues in the fusion of ^{12}C with ^{181}Ta and ^{197}Au and of ^{16}O with ^{165}Ho and ^{181}Ta have been measured at incident energies varying from the Coulomb barrier up to about 10 MeV/nucleon. The cross sections for fusion of these ions without fission have been deduced and they show that such a process may only occur for projectile angular momenta smaller than a critical value. The excitation functions for individual reactions provide evidence for the emission of preequilibrium nucleons during the thermalization of the composite nucleus and may be satisfactorily reproduced by a calculation based on the Boltzmann master equation theory.

PACS number(s): 25.70.Jj, 25.70.−z

I. INTRODUCTION

This paper is devoted to the study of the fusion of ^{12}C and ^{16}O ions with heavy nuclei at low incident energies, below 10 MeV/nucleon. This investigation is part of a comprehensive study, made by the activation technique, of the reactions induced by these ions on heavy nuclei. The experiments we made include the measurement of a great number of excitation functions, of recoil range distributions, and of the angular distributions of radioactive residues. In all the experiments we made, which are listed in Table I, we have been able to measure the cross sections of many reactions, corresponding to a large fraction of the reaction cross section. The analysis of these data, many of which have not yet been published, shows that, even at such low energies, incomplete fusion reactions compete with fusion with a rather large probability [1–6]. However, in this paper we will discuss the fusion reactions, which are interesting for several reasons. As shown in Sec. II, in all the considered cases, we have been able to measure the cross section for the *fusion* of the projectile with the target *without subsequent fission*. As in our previous works [1–6], this cross section will be indicated by the notation $\sigma_{CF}[1-P_F]$ where the subscript CF means complete fusion and P_F is the fission probability. This cross section first increases quite rapidly, reaches a maximum, and then starts to decrease following approximately a $1/E$ law, where E is the projectile-target relative energy in the center of mass system. This indicates the existence of a critical angular momentum L_{part}, above which fusion leads to fission. In Sec. III, we will also show that the excitation functions for production of fusion residues provide evidence for the emission of preequilibrium nucleons during the thermalization of the composite nucleus created in the fusion process and we will discuss a quantitative theoretical description of this reaction mechanism. Finally, Sec. IV contains our conclusions.

II. EXPERIMENTAL RESULTS

In the interaction between ^{12}C and ^{16}O and heavy nuclei, the heavy residues with charge equal to or one unit less than Z_{CN}, the sum of the projectile and the target charges, are produced in the fusion reaction. This is proved by recoil range measurements which show that these residues recoil with a velocity corresponding to the full momentum transfer [1] and, as will be shown later, by the measurement of their angular distributions which shows that they recoil in a narrow forward cone.

The sum of the cross sections for production of these residues is the dominant contribution to $\sigma_{CF}[1-P_F]$. A minor contribution also comes from the production of residues with two charge units less than Z_{CN}, which at the energies we consider in this paper, is usually less than about 15% of $\sigma_{CF}[1-P_F]$ [2–4].

In the case of the interaction of ^{12}C with ^{197}Au and ^{181}Ta, a discussion of the experiments and of the evaluation of $\sigma_{CF}[1-P_F]$ is given elsewhere [2–4] and will not be repeated here where, for the two cases considered, we simply show in Fig. 1 $\sigma_{CF}[1-P_F]$ as a function of the incident energy.

TABLE I. In column 1 are listed the reactions we have investigated; in columns 2 and 4 the energy intervals (in MeV) over which the measurements of the excitation functions and the angular distributions extend. Column 3 gives the energies (in MeV) at which the recoil range distributions have been measured.

Reaction	Excitation functions (MeV)	Recoil ranges (MeV)	Angular distributions (MeV)
$^{12}C+^{181}Ta$	54.0–98.0	77.36	
$^{12}C+^{197}Au$	57.0–97.0	120.0	
$^{16}O+^{165}Ho$	73.0–126.0		
$^{16}O+^{181}Ta$	76.0–126.0	112.0	78.0–128.0

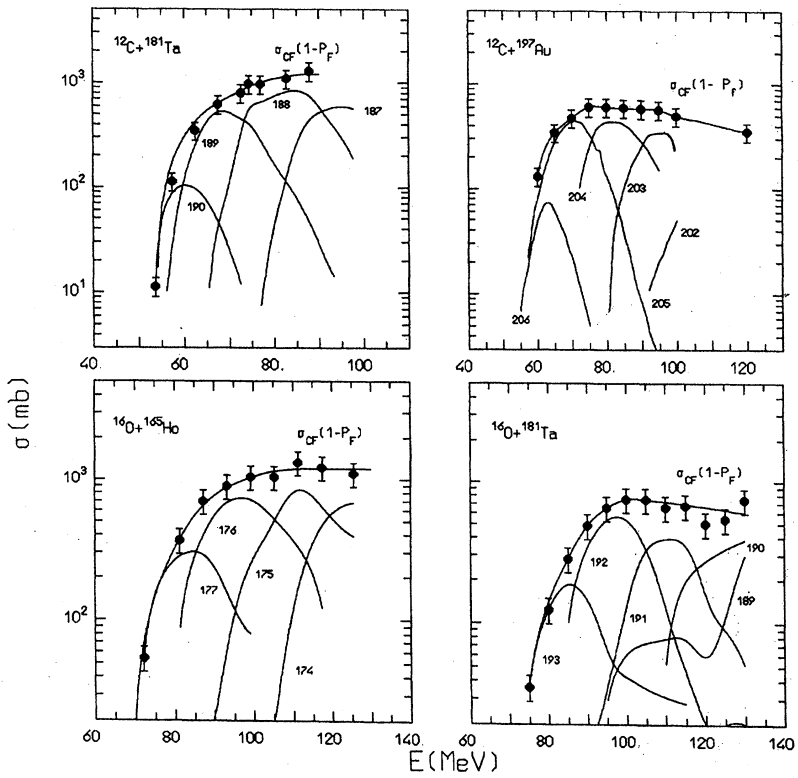

FIG. 1. The black dots give the cross sections $\sigma_{CF}[1-P_F]$ for fusion without fission for the heavy ion reactions studied. The averages of these cross sections over local fluctuations (due to the experimental uncertainty) are given by the full lines passing through the experimental points. The other full lines give the excitation functions for production of the residues with the A value shown.

The results of the experiments concerning the interaction of ^{16}O with ^{165}Ho and ^{181}Ta have not been previously published and will be briefly discussed in the following where, however, we will limit ourselves to discussing the data concerning fusion reactions. A more complete description of these experiments will be given elsewhere [7].

Both experiments have been made at the Laboratori Nazionale del Sud in Catania using the 16 MeV MP tandem accelerator. The experimental apparatus we used is described in Ref. [8].

In the case of the interaction of ^{16}O with ^{165}Ho, the cross sections for production of 20 isotopes of Re, W, Ta, Hf, Lu, Yb, and Tm have been measured at nine energies varying from about 72 to about 125 MeV by irradiating with a beam of ^{16}O, in different charge states (6^+, 7^+, and 8^+) according to the various incident energies, targets of ^{165}Ho of thickness varying from about 800 to about 1000 $\mu g/cm^2$ followed by an aluminum catcher of about 800 $\mu g/cm^2$. The beam intensity varied from about 30 e nA for the 8^+ charge state to several hundred e nA for the 6^+ charge state. The irradiation times varied from 30 min to a few hours according to the beam intensity and the half-lives of the isotopes that were expected to be produced with the highest intensity at the different energies. Since the irradiation times were comparable to or even longer than the half-lives of some of the isotopes produced, the fluence of the oxygen beam was monitored every 30 s to allow one to take into account the fluctuations in the beam intensities in evaluating the production cross sections. After the irradiations, the γ-ray activities induced both in the Ho targets and in the Al catchers were counted for several weeks using HPGe counters with efficiency varying from 25–30 to 75–80 %. The detector efficiencies were measured with calibrated ^{152}Eu sources before starting the counting of the activity and periodically checked during the several counting weeks. The ^{152}Eu and ^{60}Co spectra, also measured periodically, were used to check the energy resolution and the stability of the electronics. The γ-ray spectra thus obtained have been analyzed with the codes GAMANAL [9] and DECDEF [10].

For this reaction, $\sigma_{CF}[1-P_F]$ is approximately given by the sum of the cross sections for production of Re and W isotopes. However, the absolute cross sections for production of many Re and W isotopes cannot be measured because the abundances of their characteristic γ-lines are either unknown or relative [11,12]. On the other hand, the cross sections for production of Ta isotopes (whose half-lives, spins and parities, characteristic γ lines, and abundances are given in Table II) can be easily measured (their values are given in Table III) and can be used to estimate $\sigma_{CF}[1-P_F]$. To do that one must observe that the Ta isotopes may be produced both directly (independently) and by decay of their higher charge Re and W isobars. The comparison of the shape of the excitation function for production of ^{177}Ta, ^{176}Ta, and ^{175}Ta with that of the corresponding W isobars which are their immediate precursors shows that these Ta isotopes are not produced independently, but only by precursor decay, and the same procedure shows that, above about 100 MeV, ^{174}Ta is also mainly produced by precursor decay.

As shown in the Appendix, the analysis of the decay curves of the activity of residues produced cumulatively, i.e., both independently and by precursor decay, gives a cross section which is a rather complicated sum of the production cross sections of the observed residue and of the cross sections for production of its precursors multiplied by factors

TABLE II. Half-lives, spin, and parity of Ta isotopes and energies and abundances of their characteristic γ lines.

Isotope	Half-life (h)	J^{π}	E_{γ} (keV)	Abundance (%) Browne and Firestone [12]
^{177}Ta	56.64	$\frac{7}{2}^{+}$	113.0	7.2
^{176}Ta	8.08	1^{-}	710.5	5.2
			1159.3	24.6
			1190.2	4.4
			1341.3	3.2
^{175}Ta	10.5	$\frac{7}{2}^{+}$	266.9	10.3
			348.5	11.4
^{174}Ta	1.04	3^{+}	206.0	57.7
			764.8	1.26
			1205.9	4.8
			1228.3	1.4

which may be greater than unity and depend both on the branching ratios for the decay of the precursors to the residue considered and on the half-lives of the precursors and the residue. As in our previous papers [1,3,4] we call these cross sections *cumulative cross sections*. In the case of the Ta isotopes these cross sections are given in Table IV. On the basis of the previous discussion and the expressions of the cumulative cross sections given in this table, we assume that, in the case of the interaction of ^{16}O with ^{165}Ho, up to about 120 MeV,

$$\sigma_{\mathrm{CF}}[1-P_F]_{^{16}\mathrm{O}+^{165}\mathrm{Ho}} \approx \sigma^{C}_{^{177}\mathrm{Ta}}/1.095+\sigma^{C}_{^{176}\mathrm{Ta}}/1.406+\sigma^{C}_{^{175}\mathrm{Ta}}/1.061+\sigma^{C}_{^{174}\mathrm{Ta}}/1.896. \quad (1)$$

This cross section is shown in Fig. 1 as a function of the incident oxygen energy.

Considering the uncertainty in the target thickness, due to local thickness fluctuations, in the measurement of the beam fluence, in the counting efficiency due to the electronics dead time, and in the statistical errors in evaluating the γ-line intensity and the background subtraction, we may estimate that the values of the cross sections for individual reactions and of $\sigma_{\mathrm{CF}}[1-P_F]$ are known with a random error of about 15%. There may be in addition a systematic error of about 5% due to the abundance of the characteristic γ lines and the estimate of the detector efficiency.

TABLE III. Cross sections for production of Ta isotopes in the interaction of ^{16}O with ^{165}Ho.

E_{lab} (MeV)	$\sigma_{^{177}\mathrm{Ta}}$ (mb)	$\sigma_{^{176}\mathrm{Ta}}$ (mb)	$\sigma_{^{175}\mathrm{Ta}}$ (mb)	$\sigma_{^{174}\mathrm{Ta}}$ (mb)
72.16	59.2		2.8	
81.21	307.3	118.8	5.5	18.5
87.23	313.4	562.7	8.8	16.3
93.18	168.5	951.4	67.1	25.4
99.20	88.0	1002.4	323.9	24.9
105.23		725.1	463.7	40.0
111.25		460.5	887.6	320.0
117.42		168.5	674.4	894.7
125.51		47.4	414.6	1289.7

TABLE IV. Cumulative cross sections for production of Ta isotopes in the interactions of ^{16}O with ^{165}Ho.

Residue	Cumulative cross sections
^{177}Ta	^{177}Ta+1.095 ^{177}W+1.095 ^{177}Re
^{176}Ta	^{176}Ta+1.398 ^{176}W+1.415 ^{176}Re
^{175}Ta	^{175}Ta+1.057 ^{175}W+1.065 ^{175}Re
^{174}Ta	^{174}Ta+1.863 ^{174}W+1.928 ^{174}Re

In the case of the interaction of ^{16}O with ^{181}Ta, as shown in Table I, we have measured: (i) a set of excitation functions using a thick target and a thick catcher, (ii) the angular distributions of the radioactive residues at several incident energies using thin targets and annular catchers as described below, and (iii) the recoil range distributions of a number of residues at 112 MeV ^{16}O energy.

For the purpose of studying the fusion reactions, in this paper we will discuss the first two measurements.

In the first experiment, the excitation functions for production of 25 isotopes of Tl, Hg, Au, Pt, Ir, Os, and Re were measured between about 69 and 126 MeV incident energy using ^{181}Ta targets of about 1000 μg/cm^2 thickness and aluminum catchers about 800 μg/cm^2 thick. As in the case of the interaction of oxygen with holmium, beams of ^{16}O in three charge states (8^{+}, 7^{+}, and 6^{+}) were used. The beam intensity varied from about 25 e nA to a few hundred e nA, the irradiation times from about 1 h to several hours, and the beam fluence was monitored every 30 s.

In the second experiment, the residue angular distributions were measured using thin ^{181}Ta targets (50–60 μg/cm^2 thick) and a circular catcher of 7.5 mm diameter and thickness of about 1800 μg/cm^2 at about 17.6 mm from the target and five annular catchers at distances varying from 17.4 to 16.6 mm, 0.2 mm thick, as schematically shown in Fig. 2. With this arrangement, considering that the beam spot on the target was approximately a circle 4 mm in diameter, we have measured the activities of residues recoiling approximately in the following angular intervals: 0°–12°, 12°–20°, 20°–27°, 27°–34°, 34°–40°, and 40°–56° [at the extremes of these angular intervals, except that at 0°, the response function $F(\theta)$ of the catchers falls to 1/2 of the maximum value].

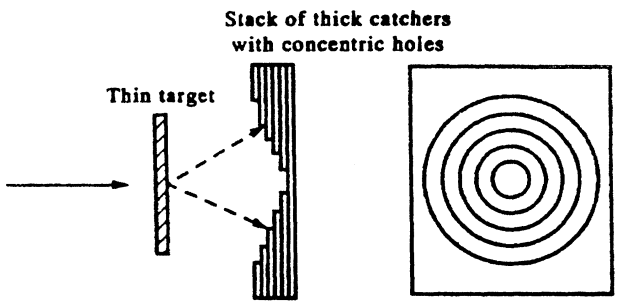

FIG. 2. Target and catcher arrangement used in the angular distribution measurements.

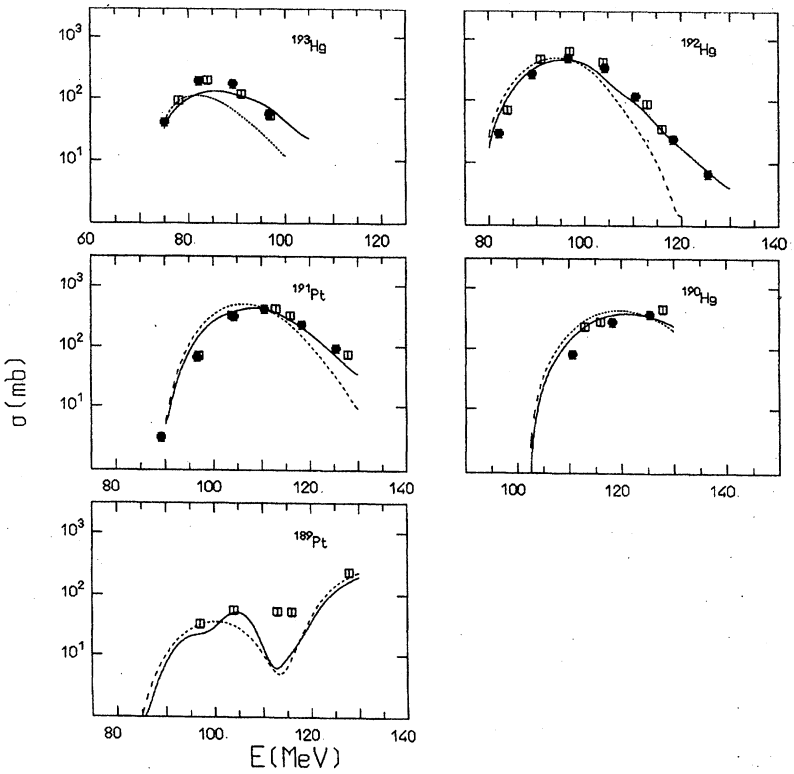

FIG. 3. Comparison of the experimental excitation functions for production of ^{193}Hg, ^{192}Hg, ^{191}Pt, ^{190}Hg, and ^{189}Pt in the fusion of ^{16}O with ^{181}Ta (the black dots are the cross sections measured with the thick target–thick catcher arrangement, the open squares those measured with the central circular detector in the angular distribution measurements) with those calculated taking into account (full lines) and without taking into account (dashed lines) preequilibrium emission.

A calculation shows that most of the residues of fusion reaction recoil in a forward cone of width less than 10°, while those produced in incomplete fusion reactions recoil to larger angles with respect to the beam direction so that they are caught by the annular catchers. We found, in fact, that the Tl and Hg isotopes were almost completely caught by the central circular catcher, together with a few lower charge isotopes like ^{193}Au and ^{191}Pt that are essentially produced by precursor decay. The cross sections corresponding to the activities found in this catcher agree very satisfactorily with those found in the thick target and thick catcher experiment, as shown in Fig. 3. Also a notable fraction of ^{189}Pt activity was found in the central circular catcher.

Limiting ourselves also in this case to the analysis of the fusion reactions, $\sigma_{CF}[1-P_F]$ may be estimated, from about 75 to about 130 MeV, by considering the cumulative cross sections for formation of ^{193}Hg^{m+g}, ^{192}Hg, ^{191}Pt, and ^{190}Hg and the fraction of the cross section for formation of ^{189}Pt corresponding to the activity of the central circular catcher in the angular distribution experiment, which is assumed to be a large fraction of the contribution of complete fusion to the production of this residue. The cross sections for production of ^{191}Hg cannot be directly used since the absolute abundances of the characteristic γ lines of ^{191}Hg^{g} are unknown.

The expressions for the cumulative cross sections for production of these residues are given in Table V, their half-lives, spins and parities, characteristic γ lines, and abundances in Table VI, and the cross sections for their formation in Table VII.

Considering the expressions for the cumulative cross sections given in Table V, and the fact that for each residue mass A the contribution of the higher charge isobar is dominant, we may approximately assume that

TABLE V. Cumulative cross sections for production of ^{193,192,190}Hg and ^{191,189}Pt in the interaction of ^{16}O with ^{181}Ta.

Residue	Cumulative cross section
^{193}Hg	^{193}Hg+1.09 ^{193}Tl
^{192}Hg	^{192}Hg+1.038 ^{192}Tl^{m}+1.033 ^{192}Tl^{g}
^{190}Hg	^{190}Hg+1.150 ^{190}Tl^{a}+1.231 ^{190}Tl^{b}
^{191}Pt	^{191}Pt+1.048 ^{191}Au^{g}+1.048 ^{191}Au^{m}+1.061 ^{191}Hg^{m}+1.060 ^{191}Hg^{g}+1.062 ^{191}Tl^{m}
^{189}Pt	^{189}Pt+1.046 ^{189}Au^{g}+1.007 ^{189}Au^{m}+1.04 ^{189}Hg+1.04(^{189}Tl^{g}+^{189}Tl^{m})

TABLE VI. Half-lives, spin, and parity of ^{193,192,190}Hg and ^{191,189}Pt and energies and abundances of their characteristics γ lines.

Isotope	Half-life (h)	J^π	E_γ (keV)	Abundance (%)
$^{193}Hg^m$	11.8	$\frac{13}{2}^+$	258.12	60.0 [13]
			407.87	25.0 [13]
			573.52	14.2 [13]
$^{193}Hg^g$	3.8	$\frac{3}{2}^-$	381.6[a]	11.0 [12]
			539.0[a]	1.2 [12]
			827.8[a]	4.0 [12].
			861.1[a]	13.0 [12]
			1040.5[a]	2.3 [12]
			1118.8[a]	8.3 [12]
^{192}Hg	4.85	0^+	157.3	7.0 [13]
			245.5	1.7 [13]
			274.87	50.4 [13]
			306.48	5.4 [13]
^{191}Pt	69.6	$\frac{3}{2}^-$	129.43	3.2 [13]
			172.22	3.52 [13]
			178.98	1.02 [13]
			268.77	1.65 [13]
			359.93	6.0 [13]
			409.48	8.0 [13]
			538.91	13.7 [13]
^{190}Hg	0.33	0^+	142.55	54.0 [13]
			171.66	3.8 [13]
^{189}Pt	10.89	$\frac{3}{2}^-$	186.67	1.32 [13]
			243.46	4.1 [13]
			300.46	2.20 [13]
			317.64	1.92 [13]
			607.60	4.8 [13]
			721.39	5.5 [13]

[a]In common with $^{193}Hg^m$.

$$\sigma_{CF}[1-P_F]_{^{16}O+^{181}Ta} \approx \sigma^C_{^{193}Hg}/1.09 + \sigma^C_{^{192}Hg}/1.04 + \sigma^C_{^{191}Pt}/1.06 + \sigma^C_{^{190}Hg}/1.18 + \sigma^{C*}_{^{189}Pt}/1.04, \quad (2)$$

where $\sigma^{C*}_{^{189}Pt}$ is the cumulative cross section for production of this isotope estimated from the activity of the central circular catcher in the angular distribution measurement. This isotope, in a complete fusion reaction, at incident energies below about 115 MeV, is mainly produced by evaporation of one α particle and four neutrons. Following the evaporation of the α the residue may recoil at an angle larger than that subtended by the central catcher. From the calculations we estimate that in a fraction of cases, decreasing from about 40% at 80 MeV to about 30% at 115 MeV, the ^{189}Pr residues are caught in the second catcher, and we have corrected for this occurrence even if, as shown in Fig. 1, the contribution to $\sigma_{CF}[1-P_F]$ of the cross section for production of this isotope is small.

As in the previous cases, we may rather safely assume that the values of $\sigma_{CF}[1-P_F]$ are known with an uncertainty of about 20% ($\approx$ 15% random and $\approx$5% systematic).

TABLE VII. Cross sections for production of ^{193,192,190}Hg and ^{191,189}Pt in the interaction of ^{16}O with ^{181}Ta. The subscript tt indicates the values measured with the thick target–thick catcher arrangement, the subscript 1° c those measured with the central catcher in the angular distribution measurement.

E_{lab} (MeV)	$\sigma_{^{193}Hg}$ (mb)	$\sigma_{^{192}Hg}$ (mb)	$\sigma_{^{191}Pt}$ (mb)	$\sigma_{^{190}Hg}$ (mb)	$\sigma_{^{189}Pt}$ (mb)
75.13	40.54_{tt}				
77.99	$91.46_{1^\circ c}$				
82.16	191.21_{tt}	28.53_{tt}			
83.95	$173.96_{1^\circ c}$	$65.57_{1^\circ c}$			
89.19	173.73_{tt}	270.15_{tt}	3.24_{tt}		
90.95	$125.67_{1^\circ c}$	$446.51_{1^\circ c}$			
96.67	56.00_{tt}	495.33_{tt}	66.13_{tt}		
96.99	$45.72_{1^\circ c}$	$606.36_{1^\circ c}$	$67.37_{1^\circ c}$		$32.29_{1^\circ c}$
103.96		$424.66_{1^\circ c}$	$323.68_{1^\circ c}$		$55.33_{1^\circ c}$
104.26		344.12_{tt}	314.95_{tt}		
110.62		118.75_{tt}	411.13_{tt}	81.47_{tt}	
112.96		$83.90_{1^\circ c}$	$412.83_{1^\circ c}$	$219.74_{1^\circ c}$	$53.18_{1^\circ c}$
115.96		$34.83_{1^\circ c}$	$325.79_{1^\circ c}$	$277.82_{1^\circ c}$	$52.52_{1^\circ c}$
118.30		23.54_{tt}	229.62_{tt}	274.47_{tt}	
125.47		6.74_{tt}	93.82_{tt}	367.70_{tt}	
127.96			$74.10_{1^\circ c}$	$454.20_{1^\circ c}$	$236.32_{1^\circ c}$

To evaluate the excitation functions of the individual reactions contributing to $\sigma_{CF}[1-P_F]$ in the four heavy ion interactions avoiding local fluctuations due to the experimental uncertainty, we have used for this quantity the values given by the full lines passing through the experimental values in Fig. 1, which are listed in Table VIII. As we have anticipated in the Introduction, the flattening and the further decrease of $\sigma_{CF}[1-P_F]$ with increasing energy, especially evident in the case of the interaction of carbon with gold, suggest the existence of a *critical* angular momentum L_{part} below which the composite nucleus created in fusion mainly

TABLE VIII. Cross sections $\sigma_{CF}(1-P_F)$ for fusion without fission for the reactions we have studied.

E_{lab} (MeV)	$^{12}C+^{181}Ta$ (mb)	$^{12}C+^{197}Au$ (mb)	$^{16}O+^{165}Ho$ (mb)	$^{16}O+^{181}Ta$ (mb)
55.00	60.0			
60.0	300.0	130.0		
65.0	540.0	343.0		
70.0	730.0	474.0		
75.0	935.0	606.0	145.0	36.0
80.0	1090.0	604.0	320.0	140.0
85.0	1190.0	594.0	545.0	281.0
90.0	1200.0	584.0	760.0	484.0
95.0	1220.0	570.0	925.0	650.0
100.0	1200.0	495.0	1050.0	746.0
105.0		460.0	1150.0	744.0
110.0		420.0	1190.0	720.0
115.0		380.0	1200.0	690.0
120.0		350.0	1200.0	660.0
125.0			1200.0	630.0
130.0			1200.0	600.0

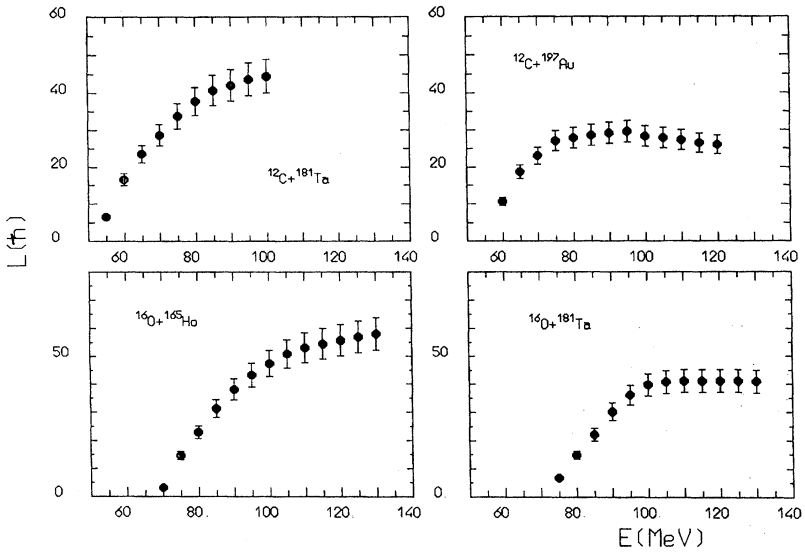

FIG. 4. Maximum angular momenta for fusion without fission, for the heavy ion interactions studied, as a function of the projectile energy.

decays by particle emission and above which it mainly fissions. If $\lambda\!\!\!^{-}$ is the de Broglie wavelength of the projectile, L_{part} may be estimated in a sharp cutoff approximation by plotting

$$L=\sqrt{\frac{\sigma_{\text{CF}}[1-P_F]}{\pi\lambda\!\!\!^{-2}}}-1 \tag{3}$$

vs the projectile incident energy. For all the reactions we have considered, the L values first increase quite quickly with energy, but soon, as shown in Fig. 4, tend to saturate to a critical value L_{part} which is given in Table IX.

The competition between particle decay and fission may in principle be explicitly considered and indeed our codes include this possibility. However, at least in part of the cases we consider, this is not possible due to the lack of accurate estimates of the fission barriers as a function of the angular momentum L. In fact their angular momentum dependence is evaluated with the rotating charged liquid droplet model (RCLDM) [13] without including any shell correction, except for $L=0$. In this case for nuclei near the magic shell regions the correction is very large, of the order of the droplet barrier itself [14]. Our data show that the shell correction cannot be neglected even in the case of rather high angular momenta. For instance, in the case of the interaction of ^{12}C with ^{197}Au, at incident energies exceeding about 80 MeV, if the fission barriers were those predicted by the RCLDM, even assuming that fission is hindered at the beginning of the deexcitation chain [15] and competes with particle decay only in the latest stages of the deexcitation chain, the atomic nuclei with the $L\geqslant 10\hbar$ could hardly survive to fission and the values of $\sigma_{\text{CF}}[1-P_F]$ would be much smaller than those we measured. The same conclusion holds in the case of the interaction of ^{16}O with ^{181}Ta. Thus, to obtain reliable results, we are obliged to use in the following calculations the sharp cutoff approximation, however drastic it may appear. Later on we will discuss the influence that this approximation may have on the results we obtain.

TABLE IX. Critical angular momenta for fusion without fission.

Reaction	Most fissile isotopes	L_{part}
$^{12}C+^{181}Ta$	Au	45±5
$^{12}C+^{197}Au$	At	28±3
$^{16}O+^{165}Ho$	Re	58±6
$^{16}O+^{181}Ta$	Tl	41±5

III. ANALYSIS OF THE EXCITATION FUNCTIONS OF THE INDIVIDUAL REACTIONS CONTRIBUTING TO THE FUSION CROSS SECTIONS

Figures 3 and 5–7 show some of the excitation functions for complete fusion reactions in the heavy ion interactions we have studied. Most of these excitation functions have a similar behavior: a rapid rise above the threshold, a rather wide maximum, and a steep decrease after the maximum. They have a width considerably larger than that of the excitation functions of reactions induced by light particles producing composite nuclei (CN) with comparable excitation energy, confirming the observation first made by Alexander and Simonoff in their study of the excitation functions of (^{12}C,xn) and (^{16}O,xn) reactions on rare-earth nuclei [19,20]. If one assumes that all these reactions proceed through the formation of a compound nucleus in a state of thermal equilibrium, the broadening of the excitation functions of heavy ion reactions may be a consequence of the much larger angular momentum carried in by the heavy ions. This causes a substantial enhancement of γ emission at the end of the evaporation cascade when particle emission is hindered by the lack of high angular momentum states of low energy. However, to reproduce the observed broadening of the heavy ion excitation functions one has to assume that the γ emission is enhanced much more than that expected on the basis of these considerations. As a matter of fact, the γ-decay rates of the compound nucleus states with energy about 10 MeV greater than that of the yrast line states must be enhanced by about a factor 100 with respect to the γ-decay rates of the neutron resonances [21].

However, this explanation seems to fail when the CN cre-

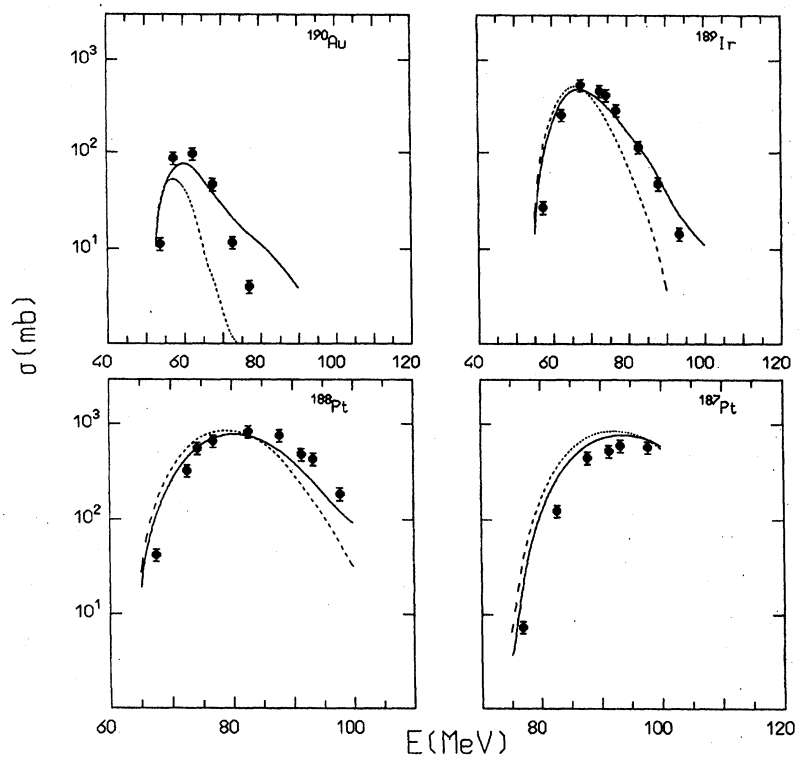

FIG. 5. Comparison of the experimental excitation functions for production of ^{190}Au, ^{189}Ir, ^{188}Pt, and ^{187}Pt, in the fusion of ^{12}C, with ^{181}Ta (black dots) with those calculated taking into account (full lines) and without taking into account (dashed lines) preequilibrium emission.

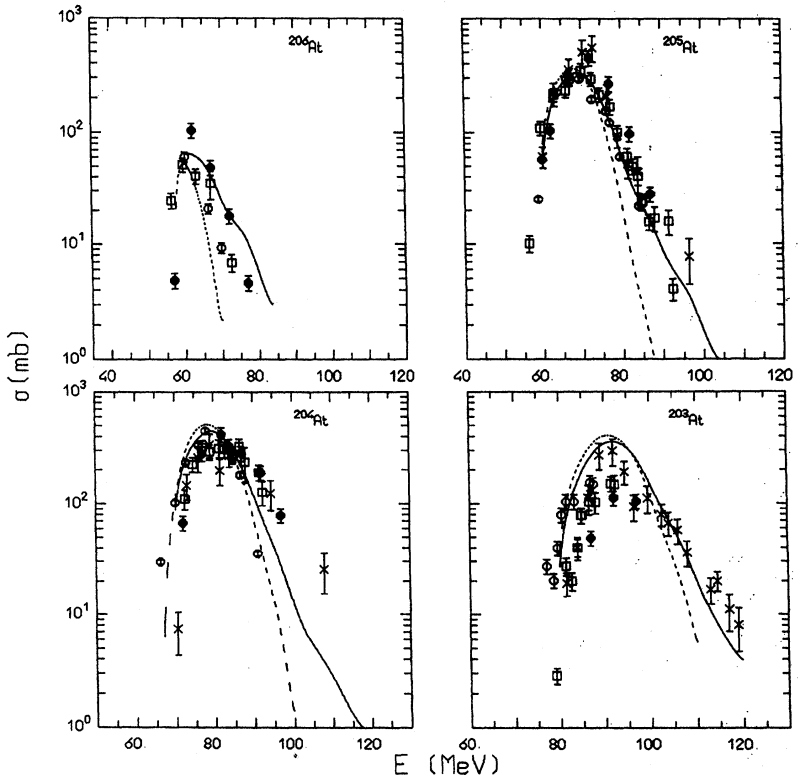

FIG. 6. Comparison of the experimental functions for production of ^{206}At, ^{205}At, ^{204}At, and ^{203}At in fusion of ^{12}C with ^{197}Au (black dots [3], open squares [16], crosses [17], and open circles [18]) with those calculated taking into account (full lines) and without taking into account (dashed lines) preequilibrium emission.

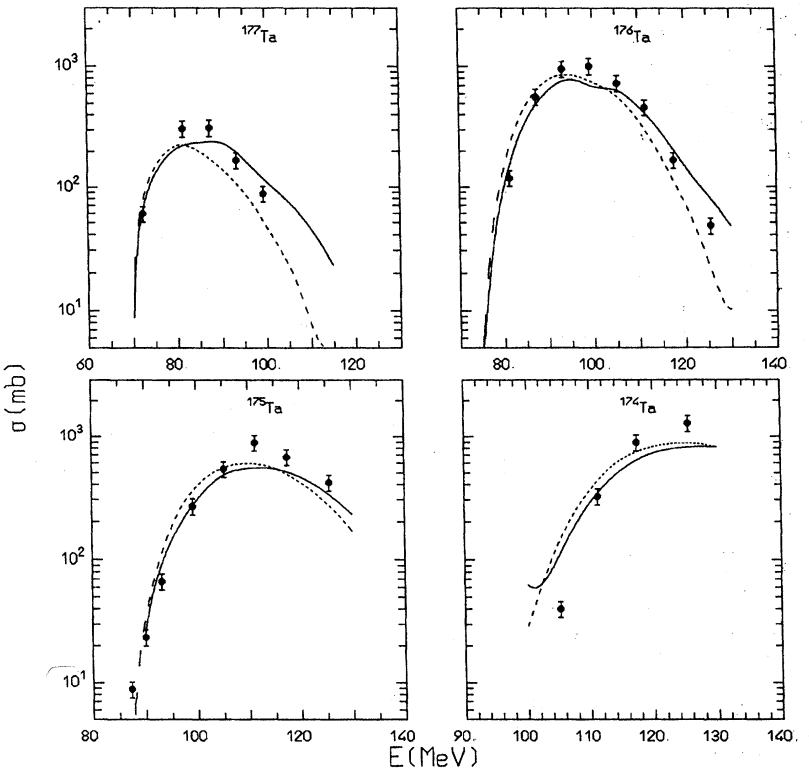

FIG. 7. Comparison of the experimental excitation functions for production of ^{177}Ta, ^{176}Ta, ^{175}Ta, and ^{174}Ta in the fusion of ^{16}O with ^{165}Ho (black dots) with those calculated taking into account (full lines) and without taking into account (dashed lines) preequilibrium emission.

ated in the fusion of the projectile with the target is sufficiently heavy, as it is in the case of the interaction of ^{12}C with ^{197}Au. In this case, as we have seen, the decay of the CN states with angular momentum exceeding about $28\hbar$ ends in a fission [3], and the evaporation residues are only produced in the decay of states with angular momenta comparable to those of the nuclei excited in reactions induced by α particles of a few tens of MeV, whose decay may be satisfactorily explained without requiring such enormous enhancement of γ emission [21]. Thus an alternative explanation is likely.

When the two heavy ions collide, the orderly translational motion of the nucleons of the projectile and the target transforms gradually into chaotic thermal motion mainly through a sequence of two body interactions. This thermalization process ends when the CN reaches a state of thermal equilibrium. During the thermalization it may happen that single nucleons, or clusters of nucleons, which still possess a quite considerable energy, are ejected into the continuum. These are called *preequilibrium* emissions. Once the thermal equilibrium state is reached, the accumulation of sufficient energy on a single nucleon or a cluster of nucleons may only occur by a random and improbable sequence of events and thus requires much longer emission times favoring the emission of low energy particles. The preequilibrium emissions lead naturally to an increase of the width of the excitation functions since they reduce quite considerably the CN excitation energy and so the number of particles which are subsequently evaporated. Thus, the cross section for emission of a given number of nucleons may be still measurable at energies where a pure evaporative process greatly favors the emission of a larger number of nucleons.

The events which may occur during the thermalization of the CN may be predicted if one assumes that this process is also governed by statistical laws. This may be done by solving a system of coupled Boltzmann master equations which describe how the energy distribution of the nucleons of the CN evolves with time as a consequence of the statistical competition of nucleon-nucleon interactions and emissions of particles into the continuum. This theory was first proposed by Harp, Miller, and Berne [22] and was extensively used by Blann and co-workers [23] in the analysis of heavy ion reactions.

Here we use the version of the theory worked out by our group and described in Refs. [24–26]. This approach has been used to analyze the excitation functions for production of At and Po isotopes in the interaction of ^{12}C with ^{197}Au [3] by considering the two interacting ions as two Fermi gases, with Fermi energy of 40 MeV, boosted by their translational momenta in the two ion center of mass system. It is assumed that, when these ions fuse, they merge into an excited CN whose further evolution is evaluated using the Boltzmann master equation theory. This approach led to a satisfactory reproduction of the broadening of the excitation functions showing that this is mainly due to the outcome of the preequilibrium emission. Further calculations made with the same approach, but reducing the Fermi energy to 35 MeV, gave a still better reproduction of these and other fusion reaction excitation functions [6], even if in both these two papers [3,6] it was suggested that the emission of preequilibrium nucleons was somewhat overestimated at the lowest considered incident energies (from 60 to 80 MeV).

Nevertheless, in spite of the success of these calculations we wish to eliminate some of the approximations made and

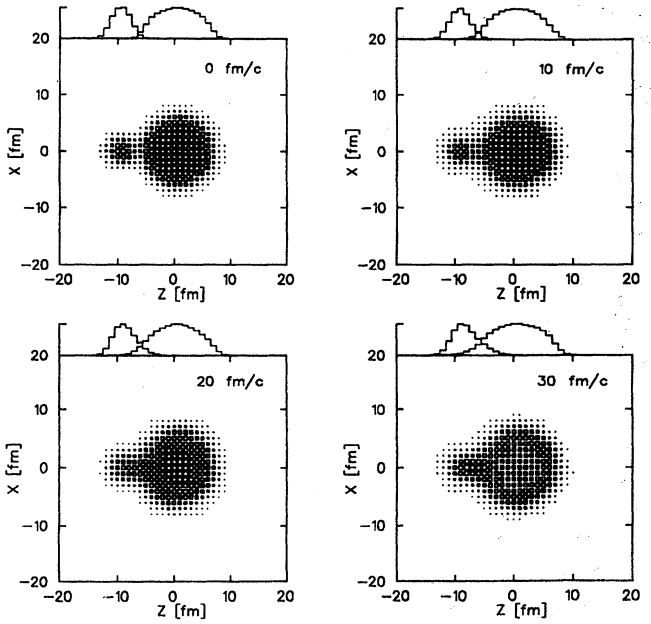

FIG. 8. Time variation (in fm/c) of the nucleon density plots in the reaction plane and of the projectile and target density profiles predicted with the Vlasov approximation for the central collision of ^{12}C with ^{197}Au at an incident energy of 80 MeV. The axis origin is chosen to coincide with the center of mass of the dinuclear system. The box sizes are proportional to the local density.

give a more realistic description of the effect of the mean field acting between the two ions, which dominates until the nucleons of the projectile and the target start to interact individually. This may be obtained by solving the Vlasov-Uehling-Uhlenbeck equation in its Vlasov limit [27].

These calculations show that at incident energies of a few tens of MeV/nucleon the mean field produces an acceleration of the centers of mass of the two colliding ions once they come in contact [28,29]. On the other hand, at the low incident energies we consider here, the same calculations show that the two ions are so greatly slowed down by the Coulomb repulsion that, since the internal motion is much faster than the collective one, they start to exchange nucleons as soon as they come in contact (thus making effective the two body interactions) and have not yet merged in a common potential well but still form a dinuclear system with a large part of the total energy (of the order of the Coulomb barrier between the two ions) in the form of collective deformation energy. This is suggested by the nuclear density plots and the projectile and target density profiles, calculated using the method of Ref. [30], which are shown in Fig. 8 for the head-on collision of ^{12}C with ^{197}Au at an incident energy of 80 MeV. Calculations at an incident energy of 130 MeV provide similar results. In agreement with this observation, to describe the thermalization of the CN with the Boltzmann master equation theory, the initial distribution of the projectile and target nucleons was calculated by coupling the translational momenta of the two ions, after they have been slowed down by the Coulomb repulsion, with their internal momenta within each ion. The internal momenta were assumed to have a Saxon-Woods distribution of the type

TABLE X. Parameters used to calculate the nucleon internal momentum distributions with a Saxon-Woods shape. In column 1 are listed the nuclei of interest in this work; in columns 2 and 3 the values of p_0 and Δp.

Nucleus	p_0 (MeV/c)	Δp (MeV/c)
^{12}C	202.56	21.30
^{16}O	207.27	21.30
^{165}Ho	250.69	11.04
^{181}Ta	251.82	10.66
^{197}Au	252.76	10.38

$$\rho(p)=\frac{\rho_0}{1+\exp[(p-p_0)/\Delta p]}\,. \tag{4}$$

In the case of light nuclei, for p_0 and Δp we have adopted the values, already used in the analysis of higher energy data, calculated as discussed in [28,29]. The shape of the excitation functions of the fusion reactions was found to depend rather critically on the value of Δp used for the momentum distribution of the heavy target nuclei and to reproduce the data required for this quantity values significantly smaller than those we used in the analysis of higher energy data, which were evaluated *a priori* by fitting the shell model momentum distributions. The parameters p_0 for these nuclei were further chosen so as to reproduce the total kinetic energy of the target nucleons as calculated with the shell model using the Becchetti-Greenless potential [31]. The values of p_0 and Δp we have used are given in Table X. We have repeated the calculations of the spectra analyzed in our previous works [28,29] with values of p_0 and Δp, for the momentum distributions of heavy nuclei, consistent with those given in Table X and we have found that the results we already got do not change significantly.

Solving the system of Boltzmann master equations one evaluates as a function of time the multiplicity and the energy distribution of the nucleons and the clusters emitted during the thermalization of the CN. If the total multiplicity of the particles emitted in a given interval of time is sufficiently small compared with unity, it may be considered equal to the probability of emitting one particle and the partial multiplicities may be considered equal to the probabilities of emitting the corresponding particles [1]. In this way one may adopt well known Monte Carlo techniques to evaluate the probability of emitting a given number of particles during the thermalization phase and the energy they carry off [32]. Our previous studies have indicated that the thermalization phase is over in less than 5×10^{-22} s from the beginning of the thermalization cascade. At the low incident energies we consider here, to use the Monte Carlo technique it is found sufficient to divide this interval of time into two parts and the only particles that are found to be emitted in appreciable numbers are neutrons, protons, and α particles. The variation of the CN angular momentum due to the preequilibrium particle emission is evaluated as described in Ref. [3]. At the end of a possible sequence of events during the thermalization cascade, a nucleus with a given Z and N, excitation energy E, and angular momentum J is formed.

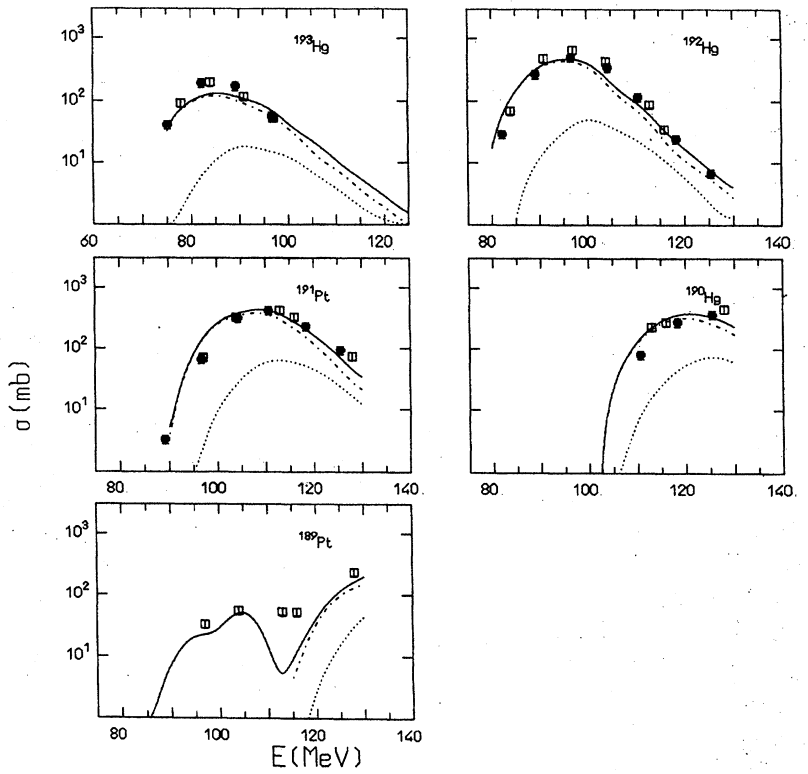

FIG. 9. Contribution of (xn) (dash- dotted lines) and $p(x-1)n$ emissions (dotted lines) to the calculated excitation functions for production of fusion reaction residues in the interaction of ^{16}O with ^{181}Ta (full lines). The black dots and the open squares give the experimental values.

The further chain of evaporations which may occur is still evaluated by the Monte Carlo approach described in Ref. [3].

The excitation energy of the composite nuclei produced in the heavy ion reactions we have studied is comparable to that of the composite nuclei formed in many reactions induced by energetic light projectiles, and the nuclei which are excited are not too far from the β stability valley, compared with those excited in many light projectile reactions. The main difference is the much higher angular momenta involved in some of the present reactions. In such conditions, we do not expect that the level density parameters and the pairing and binding energies entering the calculation are different from those used by general agreement in the analysis of light particles induced reactions [33] and thus we have decided *a priori* to use the following.

(a) The level density parameter $a=A/8$ MeV^{-1} for nuclei far from the magic shell region $Z\approx 82$ and $N\approx 126$. For nuclei with $78<Z<86$ and $124<N<128$, below $\approx$ 20 MeV, a was linearly reduced with decreasing energy from the value $A/8$ MeV^{-1} to the value

$$a(Z,N)=\frac{A}{8}-(5.52-1.38|Z-82|)-(8.48-2.12|N-82|)\ \text{MeV}^{-1}, \quad (5)$$

which, looking at the published data [33], we estimate to hold at the slow neutron resonance energy B_n.

(b) The experimental binding energies [34].

(c) The Nemirovski and Adamchuck pairing energies [35].

We have also decided to use a consistent model to evaluate the quantities on which the angular momentum effects mostly depend. The yrast state energies as a function of J were evaluated with the RCLDM using the BARFIT code [13] and the moments of inertia of excited nuclei with the MOMFIT code [13]. The calculations were made using the sharp cutoff approximation as discussed in Sec. II; however, the influence that this approximation may have on our conclusions is discussed below.

The calculations (given by the full and the dashed lines) are compared with the experimental excitation functions (given by the black dots, the open squares, the open circles, and the crosses) in Fig. 3 and Figs. 5–7. The calculations made by taking into account the emission of particles during the thermalization and before reaching the statistical equilibrium are given by the full lines; those made neglecting the emission of preequilibrium particles are given by the dashed lines. These comparisons seem to confirm the need to take into account the possibility of preequilibrium emissions during the thermalization of the CN. Neglecting this possibility often gives a systematic disagreement with the data. The comparison of some of these results with those obtained in our previous calculations [3,6] shows that the agreement of the theory with the experimental data is generally improved, especially at the lowest incident energies.

A few comments may help to judge the quality of the agreement between the calculation and the experiment.

(a) Even if in most cases the measured excitation functions give as a function of the incident energy the cumulative yield of xn and $p(x-1)n$ emissions, the contribution of the xn emissions is the dominant one. This is shown as an example in Fig. 9 for the excitation functions of the reactions produced in the interaction of oxygen with tantalum. The dash-dotted lines give the contribution of the (^{16}O,xn) reac-

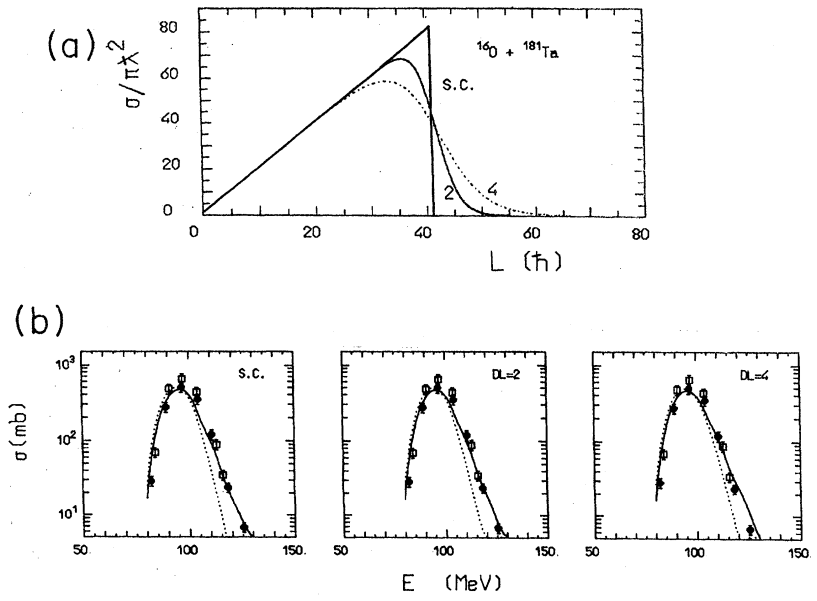

FIG. 10. (a) Comparison of the sharp cutoff (S.C.) cross section $\sigma_{CF}[1-P_F]$ and those given by (7) with $\Delta L=2$ and 4. (b) Comparison of the excitation functions for production of ^{192}Hg in the interaction of ^{16}O with ^{181}Ta (black dots and open squares) with those calculated using $\sigma_{CF}[1-P_F]$ for the sharp cutoff approximation and the smooth expression (7) with $\Delta L=2$ and 4. The full lines give the calculations including preequilibrium emission and the dotted lines the calculations made without considering such a possibility.

tion and the dotted lines the contribution of the $[^{16}O,p(x-1)n]$ reaction (this is also for the case of ^{191}Pt which is produced only through precursor decay). Below about 115 MeV the dominant contribution to the formation of ^{189}Pt is due to the $(^{16}O,\alpha 4n)$ reaction. The relative contribution cf the $[^{16}O,p(x-1)n]$ reaction increases in the tail of the excitation functions since the proton is mainly emitted in the preequilibrium phase of the reaction, which mostly contributes to the tails of the calculated excitation functions. In all the cases we have considered, the $[^{16}O,p(x-1)n]$ contribution, though relatively small, contributes in a non-negligible way to improve the agreement between the data and the calculation.

(b) As discussed before, the emission of preequilibrium particles produces long tails in the excitation functions and decreases the cross section at energies between the threshold and the maximum of the excitation functions. This feature is clearly observable in most of the cases, even if the difference in the calculated cross sections in this energy interval is not large. However, when the threshold of the reaction is below the Coulomb barrier between the projectile and the target, this simple feature may be substantially altered. Let us specifically consider the case of the excitation function for production of ^{190}Au in the interaction of ^{12}C with ^{181}Ta, shown in Fig. 5. Let us write

$$\sigma_{^{190}\mathrm{Au}}(E)=\sigma_{CF}[1-P_F](E)\mathscr{P}_{3n}(E), \tag{6}$$

where $\mathscr{P}_{3n}(E)$ is the probability that, once formed, the composite nucleus ^{193}Au decays by emitting just three neutrons. The reaction threshold is, in this case, about 42.4 MeV, and $\mathscr{P}_{3n}(E)$ is expected to have a maximum at about $E\approx$ 50 MeV. The shape of the excitation function at the lowest energies depends in this case essentially on $\sigma_{CF}[1-P_F](E)$ which, as shown in Fig. 1 and in Table VIII, increases quickly with increasing energy and shifts the maximum of the excitation function to about 60 MeV. The calculations with and without preequilibrium emissions give in this case very different results because in the energy region considered we are in the tail of $\mathscr{P}_{3n}(E)$ where the two predictions mostly differ. The same considerations hold in the case of the excitation function for production of ^{206}At in the interaction of carbon with gold, shown in Fig. 6.

(c) The calculations have been made in the sharp cutoff approximation, that is, by assuming that for $L\leq L_{\mathrm{part}}$ the composite nuclei formed in a complete fusion event decay by emitting with certainty particles and γ rays, while for $L>L_{\mathrm{part}}$ they fission during their deexcitation. The reason for this procedure is, as explained before, the lack of accurate predictions of fission barriers and the sharp cutoff approximation is justified if the fission barriers decrease quickly with increasing L, as widely expected and explicitly predicted by the RCLDM [13]. However, even in presence of such a quick decrease, it is likely that particle decay will compete with fission for L values somewhat larger than L_{part} before becoming negligible, and fission may occur with a probability increasing with L for L values not much smaller than L_{part}. The effect of the sharp cutoff approximation on the calculations has been studied in the interaction of carbon with gold in a previous work [3] using for the cross section of fusion without fission the expression

$$\sigma_{CF}[1-P_F]=\pi\lambda\!\!\!^{-2}\sum_{L=0}^{L=\infty}\frac{2L+1}{1+\exp[(L-L_{\mathrm{part}})/\Delta L]}, \tag{7}$$

and it was concluded that the use of this cross section instead of the sharp cutoff cross section does not modify in an appreciable way the results of the calculations. However, in three of the heavy ion interactions we study in this work, L_{part} exceeds considerably the value found experimentally in the interaction of carbon with gold and we may ask if the situation may be different in these cases. In Fig. 10 we show how the use of (7) instead of the sharp cutoff expression modifies the theoretical excitation function for production of ^{192}Hg in the interaction of oxygen with tantalum. We have made the calculation for ΔL equal to 2 and 4. The results of

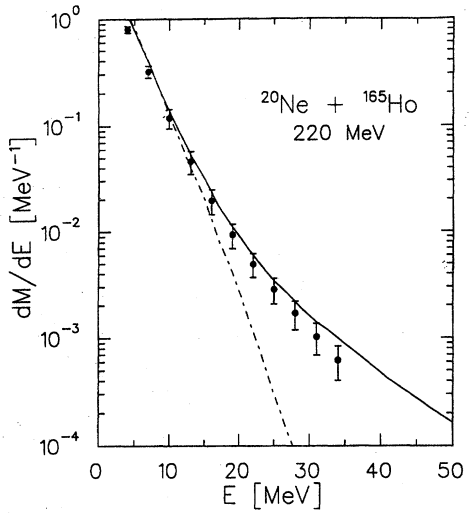

FIG. 11. Comparison of the measured spectrum of the neutrons emitted in the fusion of ^{20}Ne with ^{165}Ho at 220 MeV [36] (black dots) with those calculated taking into account (full line) and without taking into account (dashed line) preequilibrium emission.

these calculations show that the use of a smooth distribution like (7) does not modify our conclusions at least when the value of ΔL is not too big. On the other hand, assuming that fission may effectively compete with particle emission for L values down to $10\hbar$ and that particle decay may compete with fission up to L values of the order of $(60–70)\hbar$ (according to the RCLDM, the value of L_{crit} above which the composite nucleus becomes unstable against fission is about $76\hbar$) our conclusions could be modified and pure evaporations from the compound nucleus might explain the measured excitation functions. However, these assumptions seem to be unrealistic and we feel that a much more probable explanation of our data is the assumption of preequilibrium emission of nucleons even at the low energies we consider. Certainly a fitting procedure using low fission barriers also at low L's, moments of inertia considerably smaller than those predicted by the RCLDM, thus increasing the yrast energies, and increasing by order of magnitudes the γ-ray decay widths at the end of the cascade of particle emissions, may lead to a reproduction of our data without considering preequilibrium emissions.

However, preequilibrium emission is also revealed by a hardening of the ejectile spectra and we may ask if the analysis of data of this type confirms our calculations. Reliable measurements of particle spectra at such low incident energies which may be useful for this purpose are rather scarce. One of the most frequently cited cross sections is that shown in Fig. 11, for the neutrons emitted in the interaction of ^{20}Ne with ^{165}Ho, at an incident energy of 11 MeV/nucleon, in coincidence with evaporation residues measured at 8° with respect to the incident beam with mean velocity equal to 90% of the full momentum transfer velocity [36]. The experimental spectrum is given by the black dots; the one calculated considering preequilibrium emissions, and evaluating the probability of their occurrence as discussed before, by the full line. The agreement is very satisfactory, while calculations neglecting the emission of preequilibrium neutrons cannot reproduce the hardest part of the spectrum, as shown by the dashed line.

IV. SUMMARY AND CONCLUSIONS

In this paper we have shown the results obtained in a study of the fusion of carbon and oxygen with heavy nuclei at incident energies below 10 MeV/nucleon.

The analysis of the excitation functions of individual fusion reactions suggests the presence of preequilibrium emissions even at such low incident energies. A satisfactory reproduction of these data has been obtained by means of the Boltzmann master equation approach assuming that the two body interactions start to be effective when the two nuclei, greatly slowed down by their Coulomb repulsion, still form a dinuclear system and a sizable fraction of their energy is frozen as collective deformation energy.

In the absence of a reliable way of obtaining the parameters describing the properties of nuclei at high excitation and at high angular momenta, which cannot be observed directly but only guessed by studying their decay, the conclusion of our study is subject to some uncertainty. We are aware of that and we therefore tried to minimize any arbitrariness in the interpretation of the data by choosing parameters widely used in the analysis of light particle reactions which produce nuclei of comparable mass and excitation energy, using the prescriptions of the rotating charged liquid droplet model to evaluate the nuclear shapes, the collective energies, and the spin distributions, and finally using a model for describing the nuclear thermalization which also reproduces well the spectra of the preequilibrium particles at higher excitation energies where the importance of preequilibrium phenomena cannot be mistaken.

Finally, let us comment on the use of the activation technique in such investigations. One of the advantages the method offers is the possibility of separating the different contributions to the reaction cross section. In this paper we have measured the cross section for fusion without fission. In other experiments [3,4] we have obtained information on incomplete fusion processes. However, the fact we wish to stress here is that the phenomenon we have investigated (the presence of preequilibrium emissions at low incident energies) could hardly be studied using a different experimental method. For instance, the cross section for production of ^{190}Au in the interaction of carbon with tantalum and for production of ^{206}At in the interaction of carbon with gold, shown in Figs. 5 and 6, appears at about 80 MeV more than one order of magnitude greater than that estimated by an evaporation calculation using the parameters we have discussed above. We have attributed this to the presence of a preequilibrium emission, even if we have not been able to reproduce very accurately these data. The fact that other authors may have a different explanation does not change the fact that the activation technique has allowed one to measure accurately a contribution of a few mb to a reaction cross section of the order in both cases of a thousand mb, whose

presence indicates that something unexpected is occurring. The same result could be obtained only with a much stronger effort using other techniques, for instance, by measuring the emitted neutron spectrum in coincidence with a prompt γ line of ^{190}Au or ^{206}At.

Thanks are due to S. Filice, C. Passagrilli, G. Ciavola, and C. Marchetta for their collaboration in the experiments discussed in this work and to P.E. Hodgson for a careful reading of the manuscript and enlightening suggestions.

APPENDIX

If a precursor p is produced during the irradiation with cross section σ_p and decays with a decay constant λ_p and a branching ratio P_P to a daughter nucleus d which during the irradiation is produced with cross section σ_d and decays with decay constant λ_d, the following equations hold for $t \leq T$, where T is the irradiation time:

$$\frac{dN_p}{dt} = \sigma_p \tau \phi(t) - \lambda_p N_p , \tag{A1}$$

$$\frac{dN_d}{dt} = \sigma_d \tau \phi(t) + P_p \lambda_p N_p - \lambda_d N_d , \tag{A2}$$

where τ is the number of target nuclei per cm^2 and $\phi(t)$ is the flux of incident ions in particles per second, while for $t \geq T$:

$$\frac{dN_p}{dt} = -\lambda_p N_p , \tag{A3}$$

$$\frac{dN_d}{dt} = -\lambda_d N_d + P_p \lambda_p N_p . \tag{A4}$$

To solve these coupled decay equations, one multiplies (A1) and (A3) by $P_p\lambda_p/(\lambda_p-\lambda_d)$ and one adds these equations to, respectively, (A2) and (A4).

One thus obtains for $t \leq T$

$$\frac{d}{dt}\left(N_d + \frac{P_p\lambda_p}{\lambda_p-\lambda_d} N_p \right) = \left(\sigma_d + \frac{P_p\lambda_p}{\lambda_p-\lambda_d} \sigma_p \right) \tau\phi(t) - \lambda_d \left(N_d + \frac{P_p\lambda_p}{\lambda_p-\lambda_d} N_p \right), \tag{A5}$$

and for $t \geq T$

$$\frac{d}{dt}\left(N_d + \frac{P_p\lambda_p}{\lambda_p-\lambda_d} N_p \right) = -\lambda_d \left(N_d + \frac{P_p\lambda_p}{\lambda_p-\lambda_d} N_p \right). \tag{A6}$$

Equation (A5) shows that the quantity $C(t) = N_d + [P_p\lambda_p/(\lambda_p-\lambda_d)]N_p$ varies during the irradiation time as if it is produced with cross section $\sigma_c = \sigma_d + [P_p\lambda_p/(\lambda_p-\lambda_d)]\sigma_p$.

At the end of irradiation one thus obtains

$$C_0 \equiv C(T) = \left(\sigma_d + \frac{P_p\lambda_p}{\lambda_p-\lambda_d} \sigma_p \right) \tau \Phi_{\lambda_d}, \tag{A7}$$

where

$$\Phi_{\lambda_d} = e^{-\lambda_d T} \int_0^T \phi(t) e^{\lambda_d t} dt. \tag{A8}$$

Equation (A6) shows that at times greater than T

$$N_d + \frac{P_p\lambda_p}{\lambda_p-\lambda_d} N_p = C_0 e^{-\lambda_d t}. \tag{A9}$$

Since

$$N_p = N_p(T) e^{-\lambda_p t}, \tag{A10}$$

the number of daughter nuclei varies with time with the law

$$N_d = C_0 e^{-\lambda_d t} - \frac{P_p\lambda_p}{\lambda_p-\lambda_d} N_p(T) e^{-\lambda_p t}. \tag{A11}$$

If $\lambda_p \gg \lambda_d$, for $t \to \infty$ the second term becomes negligible in comparison with the first and

$$N_d \to C_0 e^{-\lambda_d t}. \tag{A12}$$

Thus if one reproduces this part of the decay curve by a simple exponential, one obtains the activity of daughter d at the end of the irradiation as $C(T)\lambda_d$ and the cumulative cross section as

$$\sigma_c = \sigma_d + \frac{P_p\lambda_p}{\lambda_p-\lambda_d} \sigma_p . \tag{A13}$$

The procedure is easily generalized to the case of several precursors. Thus in the case of the sequence

$$A \to B \to C$$

with decay constants

$$\lambda_A \gg \lambda_B \gg \lambda_C \tag{A14}$$

and branching ratios P_A and P_B, one obtains the cumulative cross section for production of C given by

$$\sigma_c^C = \sigma_i^C + \frac{\lambda_B}{\lambda_B-\lambda_C} \sigma_i^B P_B + \frac{\lambda_A\lambda_B}{(\lambda_A-\lambda_C)(\lambda_B-\lambda_C)} \sigma_i^A P_A P_B . \tag{A15}$$

The procedure shown does not hold (either in the case of a single precursor or in the case of several precursors) if the decay constants do not satisfy (A14), since in this case all terms contributing to $N_d(t)$ have to be considered whatever time interval is taken. This was the case for ^{176}Ta and ^{174}Ta produced in the interaction of ^{16}O with ^{165}Ho.

[1] D.J. Parker, P. Vergani, E. Gadioli, J. J. Hogan, F. Vettore, E. Gadioli Erba, E. Fabrici, and M. Galmarini, Phys. Rev. C **44**, 1528 (1991).
[2] P. Vergani, E. Gadioli, E. Vaciago, P. Guazzoni, L. Zetta, G. Ciavola, M. Jaskola, P. L. Dellera, V. Campagna, and C. Marchetta, Report No. INFN/BE 92/02, 1992 (unpublished).
[3] P. Vergani, E. Gadioli, E. Vaciago, E. Fabrici, E. Gadioli Erba, M. Galmarini, G. Ciavola, and C. Marchetta, Phys. Rev. C **48**, 1815 (1993).
[4] M. Crippa, E. Gadioli, P. Vergani, G. Ciavola, C. Marchetta, and M. Bonardi, Z. Phys. A **350**, 121 (1994).
[5] M. Cavinato, E. Fabrici, E. Gadioli, E. Gadioli Erba, P. Vergani, C. Brusati, M. Crippa, G. Colombo, S. Filice, and C. Passagrilli, in *Heavy Ion Fusion: Exploring the Variety of Nuclear Properties*, edited by A. M. Stefanini, G. Nebbia, S. Lunardi, G. Montagnoli, and A. Vitturi (World Scientific, Singapore, 1994), p. 180.
[6] E. Gadioli, P. Vergani, M. Cavinato, E. Fabrici, E. Gadioli Erba, M. Crippa, G. Colombo, I. Redaelli, M. Ripamonti, C. Brusati, G. Ciavola, C. Marchetta, and S. H. Connell, in *Proceedings of the Tours Symposium on Nuclear Physics II*, edited by H. Utsunomiya, M. Ohta, J. Galin, and G. Münzenberg (World Scientific, Singapore, 1995), p. 309.
[7] E. Gadioli *et al.* (unpublished).
[8] R. Fresca Fantoni, E. Gadioli, P. Guazzoni, P. Vergani, L. Zetta, P. L. Dellera, F. Tomasi, V. Campagna, G. Ciavola, and C. Marchetta, Appl. Radiat. Isot. **45**, 325 (1994).
[9] J. A. B. Goodall, UKAEA Report No. AERE-M3185, 1982.
[10] P. Vergani (unpublished).
[11] U. Reus, W. Westmeier, and I. Warnecke, At. Data Nucl. Data Tables **29**, 1 (1983).
[12] E. Browne and R. B. Firestone, *Table of Radioactive Isotopes* (Wiley, New York, 1986).
[13] A. J. Sierk, Phys. Rev. C **33**, 2039 (1986).
[14] W. D. Myers, *Droplet Model of Atomic Nuclei* (Plenum, New York, 1977).
[15] D. J. Hinde, Nucl. Phys. **A553**, 255 (1993), and references therein.
[16] R. Bimbot, M. Lefort, and A. Simon, J. Phys. (Paris), **29**, 563 (1968).
[17] T. D. Thomas, G. E. Gordon, R. M. Latimer, and G. T. Seaborg, Phys. Rev. **126**, 1805 (1962).
[18] S. Baba, K. Hata, S. Ichikawa, T. Sekine, Y. Nagame, A. Yokohama, M. Shoji, T. Saito, N. Takahashi, H. Baba, and I. Fujiwara, Z. Phys. A **331**, 53 (1988).
[19] J. M. Alexander and G. N. Simonoff, Phys. Rev. **130**, 2383 (1963).
[20] G. N. Simonoff and J. M. Alexander, Phys. Rev. **133**, B104 (1964).
[21] J. Gilat, E. Roger Jones III, and J. M. Alexander, Phys. Rev. C **7**, 1973 (1973).
[22] G. D. Harp, J. M. Miller, B. J. Berne, Phys. Rev. **165**, 1166 (1968); G. D. Harp and J. M. Miller, Phys. Rev. C **3**, 1847 (1971).
[23] M. Blann, A. Mignerey, and W. Scobel, Nukleonika **21**, 335 (1976); M. Blann, Phys. Rev. C **23**, 205 (1981); **31**, 1245 (1985); B. A. Remington, M. Blann, A. Galonsky, L. Heilbronn, F. Deak, A. Kiss, and Z. Seres, *ibid.* **38**, 1746 (1988); B. A. Remington, M. Blann, and G. F. Bertsch, *ibid.* **35**, 1720 (1987).
[24] E. Fabrici, E. Gadioli, E. Gadioli Erba, M. Galmarini, F. Fabbri, and G. Reffo, Phys. Rev. C **40**, 2548 (1989).
[25] I. Cervesato, E. Fabrici, E. Gadioli, E. Gadioli Erba, and M. Galmarini, Phys. Rev. C **45**, 2369 (1992).
[26] M. Cavinato, E. Fabrici, E. Gadioli, E. Gadioli Erba, M. Galmarini, and A. Gritti, Z. Phys. A **347**, 237 (1994).
[27] G. F. Bertsch and S. Das Gupta, Phys. Rep. **160**, 189 (1988), and references therein.
[28] C. Brusati, M. Cavinato, E. Fabrici, E. Gadioli, and E. Gadioli Erba, in *Proceedings of the 7th International Conference on Nuclear Reaction Mechanisms,* Varenna, 1994 [Ric. Sci. Educ. Perm. Suppl. (100) (1994)].
[29] C. Brusati, M. Cavinato, E. Fabrici, E. Gadioli, and E. Gadioli Erba, Z. Phys. A (to be published).
[30] A. Bonasera, F. Gulminelli, and J. J. Molitoris, Phys. Rep. **243**, 1 (1994).
[31] F. D. Becchetti and G. W. Greenlees, Phys. Rev. **182**, 1190 (1969).
[32] I. Dostrovsky, Z. Fraenkel, and G. Friedlander, Phys. Rev. **116**, 683 (1959).
[33] E. Gadioli and P. E. Hodgson, *Preequilibrium Nuclear Reactions* (Clarendon, Oxford, 1992).
[34] A. H. Wapstra and K. Bos, At. Data Nucl. Data Tables **19**, 175 (1977).
[35] P. E. Nemirovski and Yu. V. Adamchuck, Nucl. Phys. **39**, 551 (1962).
[36] E. Holub, D. Hilscher, G. Ingold, U. Jahnke, H. Orf, and H. Rossner, Phys. Rev. C **28**, 252 (1983).